Amplitude Characteristics of Littoral Sea Clutter Data at K-band and W-band

Samiur Rahman
SUPA School of Physics & Astronomy
University of St Andrews
St Andrews, Scotland
sr206@st-andrews.ac.uk

Aleksanteri Vattulainen
SUPA School of Physics & Astronomy
University of St Andrews
St Andrews, Scotland
av41@st-andrews.ac.uk

Duncan A. Robertson
SUPA School of Physics & Astronomy
University of St Andrews
St Andrews, Scotland
dar@st-andrews.ac.uk

***Abstract*—Sea clutter data at millimeter wave frequencies are quite limited in the literature. Recent advancements in millimeter wave radar technology have created a potential for its use in maritime surveillance and autonomy. Hence, collecting data at this frequency range is of great interest to both academia and industry. This study reports on a field trial conducted at St Andrews in winter 2020 to collect littoral sea clutter data using K-band (24 GHz) and W-band (94 GHz) radar systems. Extensive data collection was done during the trial, where this work specifically concentrates on analysis of the amplitude characteristics of the sea clutter returns. Analysis of the dataset shows that the radar backscatter was heavily dominated by sea-spikes. The modal normalized radar cross section (NRCS) values for Bragg, burst and whitecap scattering are measured to be -47, -30 and -17 dB respectively at 24 GHz in horizontal polarization and -48, -26 and -12 dB respectively at 94 GHz in circular polarization, measured at grazing angles of 1-3°. The backscatter from the smooth surface is found to be below the noise floor equivalent NRCS (-65 dB). Also, the power spectrum analysis of range-time intensity plots is discussed, revealing information on the sea surface dynamics.**

Keywords—Sea clutter, sea-spikes, breaking waves, millimeter wave, FMCW

I. Introduction

Millimeter wave radar technology has been advancing recently, mainly due to the development of chipsets at these frequencies by the automotive industry. These radars have the advantage of being compact and lightweight. The radar systems for maritime navigation traditionally operate in X-band, hence, the available sea clutter data and the subsequent analyses of them at X-band or below are quite comprehensive in the literature. Meanwhile, empirical data recorded at higher frequencies are quite scarce. In [1]–[3], where quite a lot of seminal work on radar sea clutter is reported, no empirical results beyond Ka-band are available.

In [4], littoral sea clutter data were gathered in St Andrews, Scotland using a 94 GHz Frequency modulated Continuous Wave (FMCW) scanning radar. It reported NRCS (σ^o) [3] of peak backscatter to be ~-22 dB, in linear polarization (both vertical and horizontal) and at low grazing angle (~ 2-3°). The radar architecture was not coherent, hence it did not collect any Doppler data. In [5], a stepped frequency radar operating at 91.5-97.5 GHz was used to collect sea clutter data in Qinhuangdao, China. It reported a σ^o value for the maximum observed peak of -24.5 dB. In [6], a very comprehensive trial (North Sea Sylt campaign) was reported which encompassed meteorological and oceanographic sensor data along with radar measurements at X, Ka and W bands. In terms of radar sea clutter, it presented range-time intensity plots from X and Ka-band data, but no amplitude or Doppler characteristics analysis at W-band were reported.

UK Engineering and Physical Sciences Research Council under grant EP/S032851/1.

The aim of this study is to expand on the existing dataset for sea-clutter, primarily at W-band. The motivation stems from the recent commercial interest in high frequency radar systems for future autonomous marine vessels. To map the dynamic sea surface, such vessels will require very high resolution radar sensor data, which can more easily be obtained by millimeter wave radars. Meanwhile, K-band radars are already being used by various commercial maritime surveillance systems, but radar sea clutter phenomenology study at this frequency range is still quite limited in the literature. So, data at this frequency is also desired. These vessels often operate close to the shore, so littoral sea data is of great importance. The field trial corresponding to this study is the first campaign of a project to collect and analyze sea clutter data at these frequencies and higher, where further trials are planned for the near future. The two radars used in this study are fully coherent, and a large amount of Doppler data were also obtained. However, this paper concentrates on the amplitude statistics and the Doppler results will be reported in a separate publication. Section II of this paper describes the sea-spike definitions used for this study. Section III elaborates on the specifics of the field trial setup. The amplitude characteristics calculation methods and results are discussed in Section IV, in terms of obtained σ^o distributions for different sea-spikes and power spectrum analysis in the form of ω-k plots. Further statistical analysis of the amplitude distribution is beyond the scope of this paper. Conclusions are presented in Section V.

II. Sea-spike terminologies

In [7], the physical and mathematical properties of various sea-spike components are provided. In [3], [8], the summary definitions are given which are as follows:

Bragg scattering: Occurs due to resonant scattering from the sea surface. This scattering arises mainly from capillary waves where the water wave lengths are less than 2.5 cm [3]. The resonance will depend on the radar wavelength. Technically, this is not a spike, but due to its contribution to the clutter 'spikiness', this phenomenon has been attributed as spike quite frequently in the literature [3], [8].

Burst Scattering: This is a spike without the wave breaking (i.e. scattering from the near vertical face of the wave crest). This phenomenon is short in duration (~ 200 ms) [3].

Whitecap scattering: This is radar backscatter coming from a breaking wave. Hence, the duration is longer than burst scattering, usually a few seconds [3]. It will thus have a broader, noise-like distribution in the radar signal amplitude time history for a range cell.

To detect a specific spike for σ^o calculation, we categorised the radar returns according to these definitions. Section IV further discusses the various detection parameters.

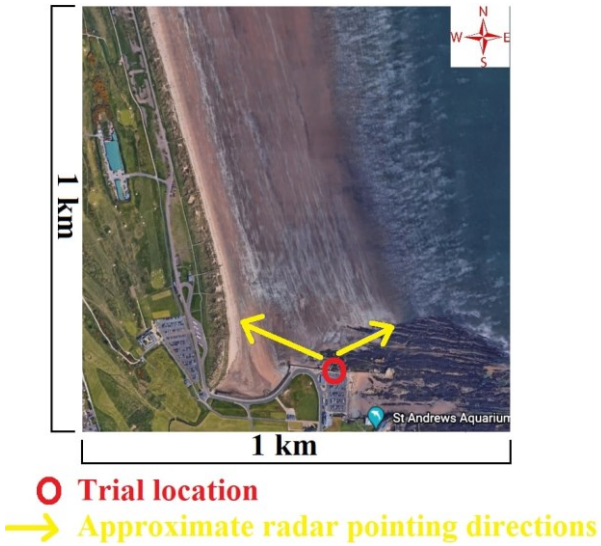

(a)

(b)

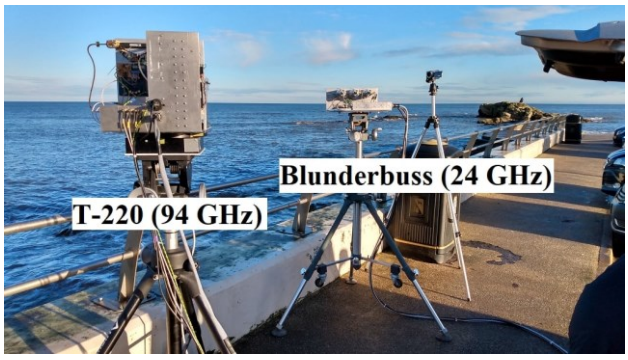

(c)

Fig.1. (a) Field trial location circled in red; (b) radars pointing ~NW towards the beach; (c) radars pointing ~NE towards the open sea

III. EXPERIMENTAL SETUP

The trial was held at the Bruce Embankment, St Andrews, Scotland on the 15th December, 2020. Fig. 1 shows the location of the trial (56˚20′41″ N 2˚48 ′06 ″ W) along with the radars' views. Fig. 1(b) shows the radars pointing ~NW towards the beach whereas in Fig. 1(c) the radars are pointing ~NE towards the open sea. The data were collected from 11:45 to 14:30 UTC. The weather was relatively clear and sunny. The wind speed was ~8 mph from the South, the temperature was 8 °C and the sea-state was 0-1 during the whole trial period, estimated by visual observation, as seen in Fig. 1(b) and (c).

Both the radars used during the trial were designed and built by the Millimetre Wave group at the University of St Andrews. The 94 GHz radar (T-220) is a very low phase noise (DDS based chirp generation), narrow fan beam FMCW radar [9]. The 24 GHz radar (Blunderbuss) is a Analog Devices™ evaluation board based, symmetric beam FMCW radar [10]. The radars are controlled from dedicated PCs, with control code software written in LabWindows™/CVI. Both radars are amplitude calibrated to within ±2 dB for NRCS measurements. Table 1 lists the key radar specifications. It should be noted that the polarizations are different for the two radars. The 94 GHz data is obtained with circular polarization (odd bounce, transmits right circular polarization and receives left circular polarization). whereas the 24 GHz data is horizontally polarized.

Both staring and azimuth-scanning mode data were collected with T-220, but only staring mode data were collected using Blunderbuss (which has a beamwidth too wide for scanning mode). This paper focuses only on the data from the staring mode operation. Data were collected by both

Table 1: 94 and 24 GHz radar specifications

Parameter	*T-220*	*Blunderbuss*
Center Frequency	94 GHz	24 GHz
Operation mode	FMCW	FMCW
Antenna beamwidth	0.92° az., 3° el.	11.2° az., 11.2° el.
Antenna gain	40.5 dBi	24.5 dBi
Polarization	Circular (odd bounce)	Linear (horizontal)
Tx power	+18 dBm	+25 dBm
Bandwidth / range resolution	750 MHz / 20 cm	250 MHz / 60 cm
Chirp time	102.026 µs	327.68 µs
Chirp repetition interval	122.34 µs	357.44 µs
Instrumented range	204.8 m	307.2 m

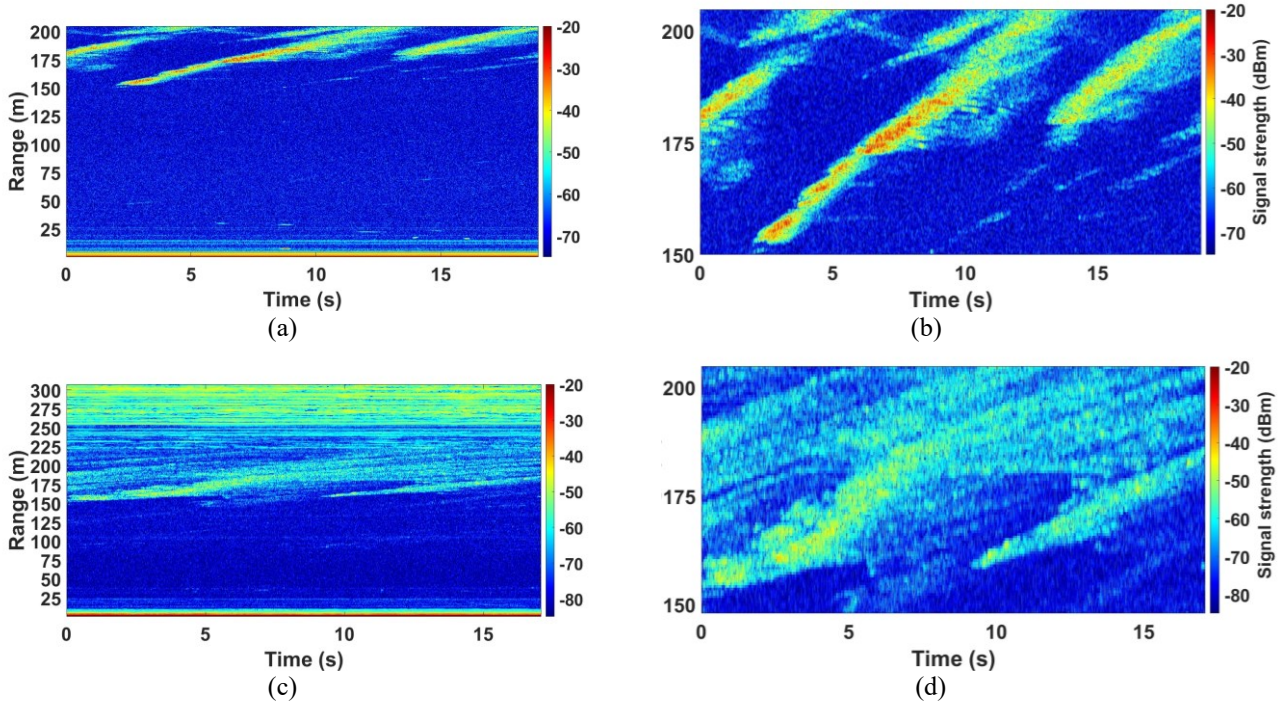

Fig. 2. Range-time intensity plots (a) 94 GHz radar looking towards the beach; (b) same plot zoomed in, showing breaking waves moving away from the radar; (c) 24 GHz radar looking towards the beach; (d) same plot zoomed in, showing breaking waves moving away from the radar

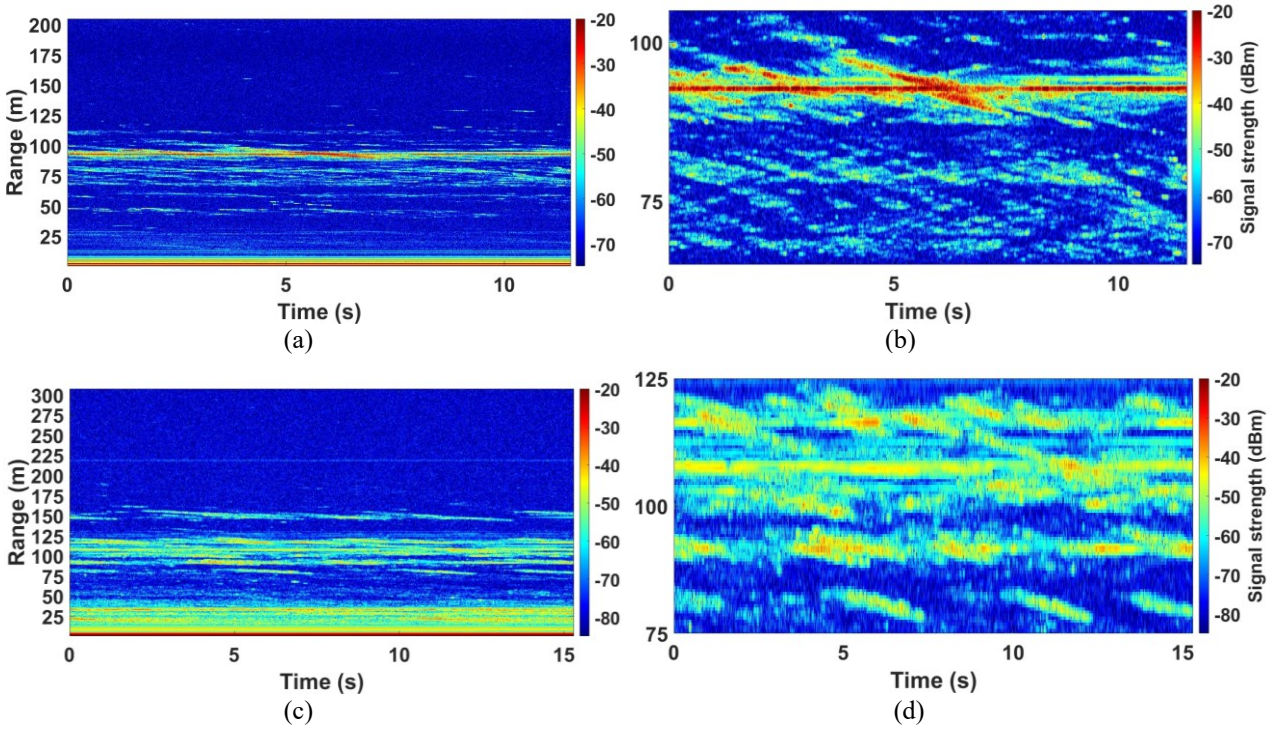

Fig. 3. Range-time intensity plots (a) 94 GHz radar looking towards the open sea; (b) same plot zoomed in, showing breaking waves moving towards the radar; (c) 24 GHz radar looking towards the open sea; (d) same plot zoomed in, showing breaking waves moving towards the radar

radars concurrently, but the instantaneous data saves were done manually from the respective PCs so are not precisely time-aligned. Prior to data collection, radar noise floors were verified by pointing them at the sky. Average noise floor levels of both the radars agreed quite well with the predicted values (-73.4 dBm for T-220 and -80.1 dBm for Blunderbuss). Data were first collected with the radars pointed ~NW at the beach (~ 220 m away) and then pointed ~NE at the sea. In the latter case, some data were also collected by pointing the radars in the direction of a protruding rock (~90 m away) to get some stationary target data. In littoral sea conditions, waves are often impacted by the submerged, semi-submerged or even protruding rocks. Hence, data were collected at different directions for clutter diversity. Note the data were

collected in shallow water littoral conditions so the amplitude characteristics are spikier than those of open sea conditions in sea-state 0-1.

The radar height above the water level as a function of time was determined by surveying the radar position with respect to the protruding rocks at low tide and accounting for the average tide height reported by the local meteorological office. The tripods were levelled and elevation angles read off from the tripod head Vernier scales. The radar height varied from 3.8 to 5.3 m during the trial.

IV. RESULTS

As the collected data set is quite extensive, we have chosen two data files for each frequency to demonstrate the experimental results. At each frequency, one file corresponds to data taken with the radars pointing ~NW towards the beach, so the waves were receding from the radar. The other file is where the radars were looking ~NE towards open sea, in which case the waves were approaching. The elevation angles were -1° for T-220 and 0° for Blunderbuss. All the data were post-processed in MATLAB®. Data associated with the results presented here are available at DOI: doi.org/10.17630/85286f40-a781-4c34-aaa3-abd6fcfb965f.

A. Range-Time Intensity Plots

Fig. 2 illustrates the range-time intensity plots generated for both 94 and 24 GHz data. The lower limits of the intensity scales correspond to the noise floors of the radars. It can be seen that there is an almost entirely negligible reflection coming from the smooth surface out to ~150 m range. Here, smooth surface means that the surface roughness level was quite low, so that no breaking wave spikes or Bragg resonant scattering were detected by the radars. The bright diagonal features correspond to waves breaking on the beach. This suggests that the radar backscatter is mainly occurring from cresting and breaking waves at sea-state 0-1 at very low grazing angles. Comparing the signal strength of the breaking waves in Fig. 2 with the average radar noise floors indicate very high SNR of 40 dB or more in some cases.

Fig. 3 shows similar range-time intensity plots, this time generated with the second file for both radars, where the waves are approaching. The presence of a large rock interrupts the continuous propagation of the waves and these combine with waves reflected from the sea wall below the radars to give a much more complex wave pattern. The water depth is slightly harder to estimate due to variable rock heights, but the average was ~3 m (based on the distance measurements done at low tide to calculate radar height). The return from the rock is clearly visible as the horizontal line in Fig. 3(b) and (d). In 3(b) for 94 GHz, it is at 92 m and the signal is very strong and stable throughout the time history as the radar beam is very narrow and that part of the rock remained above water.

In 3(d), the 24 GHz radar was pointed at a slightly different bearing and has a wider beam so the return from the rock appears at 107 m. The amplitude is not constant in successive chirps, most probably because it was being intermittently washed over by waves.

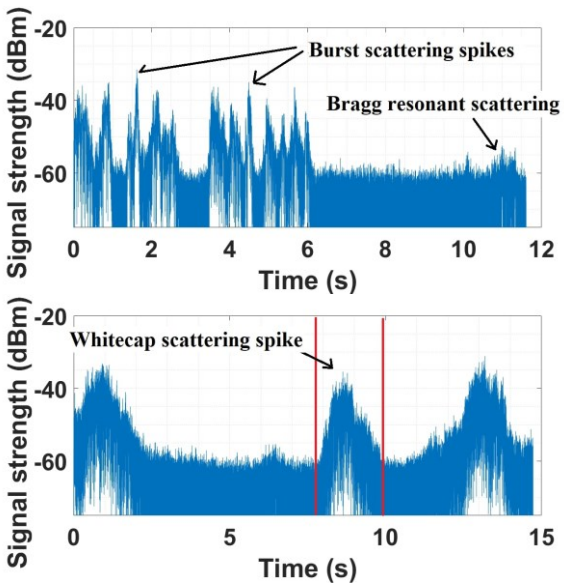

Fig. 4. Example clutter range cell time history showing specular Burst scattering spikes and Bragg scattering (top) and longer duration whitecaps (bottom)

B. NRCS Calculation

Due to the low sea-state and consequent lack of waves in open water, it has not been possible to process NRCS vs grazing angle, as most range bins contained reflection from the smooth surface below the modal value of the noise equivalent NRCS (-65 dB). Instead, NRCS values have been calculated for fixed grazing angle values where different types of spikes are present. To select different spikes, the amplitude and temporal threshold based method discussed in [11], [12] has been applied. We essentially followed that methodology to determine the regions for Bragg, burst and whitecap. In [12], the thresholds are:- i) amplitude threshold is 5 times deviation of the echo amplitude (~14 dB). Here, we have selected an amplitude threshold of 5 dB above the maximum value of the noise floor envelope, ii) minimum spike duration of 0.1 s and iii) minimum interval between spikes of 0.5 s. These were determined by careful visual inspection. Fig. 4 shows some examples of the different scattering phenomena.

Fig. 5 shows the histogram plots of the σ^o values obtained at 94 GHz for Bragg, burst and whitecap. The first two were calculated for a grazing angle of 3°, whereas the whitecap NRCS was processed for a grazing angle of 1.3°. This was done because a single grazing angle with all three scattering types was not found that satisfied the thresholds. The modal values of σ^o for Bragg, burst and whitecap are -48 dB, -26 dB and -12 dB respectively. The modal NRCS of Bragg scattering at 3° grazing angle matches quite well with the value calculated from the updated NRL model given in [2]. The whitecap modal value is quite high, which might be due to the fact that the breaking waves here were very close to the beach so they interacted more with the shore surface, increasing the return signal amplitude.

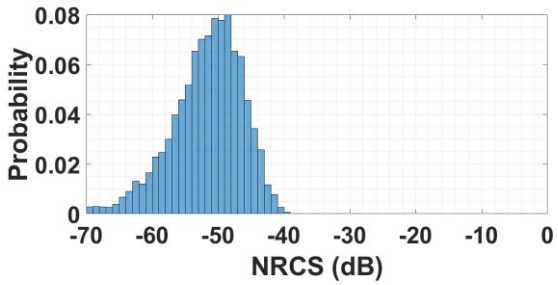

(a)

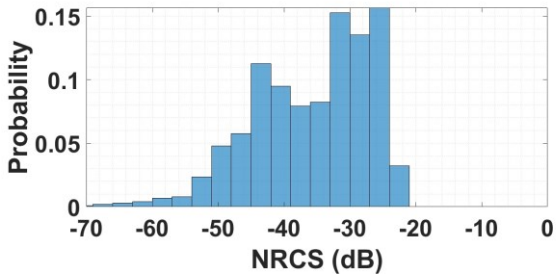

(b)

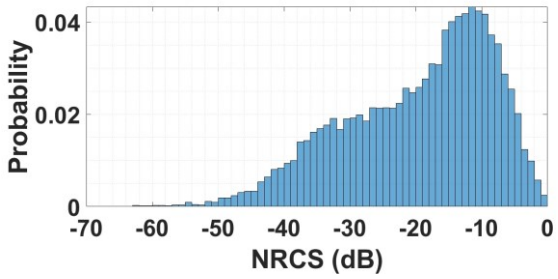

(c)

Fig. 5. NRCS histograms at 94 GHz for (a) Bragg scattering at 3° grazing angle, (b) burst scattering at 3° grazing angle, (c) whitecap scattering at 1.3° grazing angle

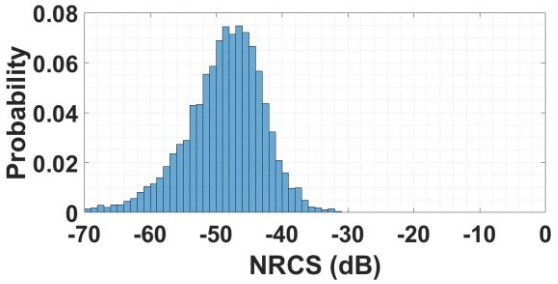

(a)

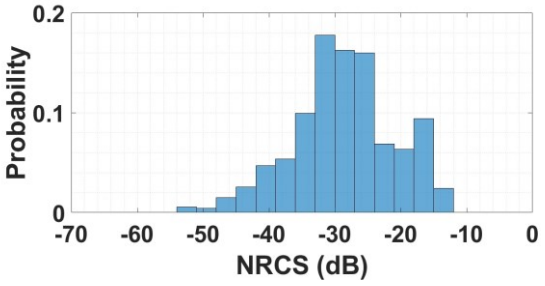

(b)

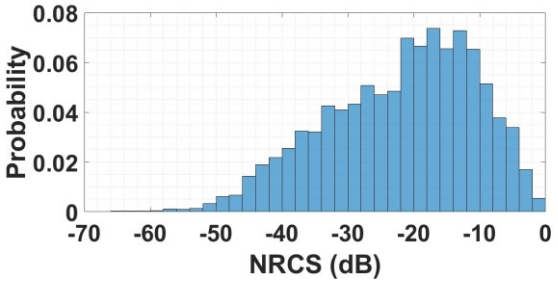

(c)

Fig. 6. NRCS histograms at 24 GHz for (a) Bragg scattering at 3° grazing angle, (b) burst scattering at 3° grazing angle, (c) whitecap scattering at 1.3° grazing angle

Fig. 6 Shows similar results for 24 GHz at the same grazing angles. The modal NRCS values here are -47 dB, -30 dB and -17 dB for Bragg, burst and whitecap respectively. The decrease in NRCS at 24 GHz is expected according to the model in [2]. It can be seen that the modal value for Bragg has not decreased, which requires further examination for thorough understanding. Currently, our hypothesis is that this could be due to the wide beamwidth of the 24 GHz radar receiving more low level energy or simply Bragg scattering resonance being more significant at lower frequency. No consistent statistical distribution fit has been found for the histograms, where perhaps more data with higher sea-states can yield a clearer statistical pattern. It should also be noted that the impact of different polarizations is not straightforward to quantify, as the two radars were operating at different frequencies. In [4], it was reported that at W-band linear polarization produced stronger returns in general, however for the strongest peaks from the breaking waves the signal strengths were similar for both polarizations. It was hypothesized that the returns became depolarized in those conditions for odd bounce circular polarisation. The NRCS values obtained in this trial however do not clearly confirm this as the calculated NRCS modal value from Bragg scattering at 94 GHz circular polarization fits the value for linear polarization predicted in [2]. This might be an intrinsic issue with littoral sea clutter data analysis as due to the shallow water conditions it is difficult to precisely determine the sea-states in a consistent manner.

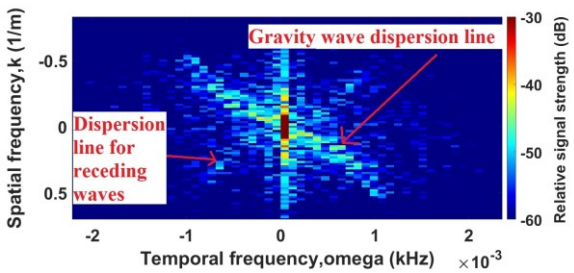

(a)

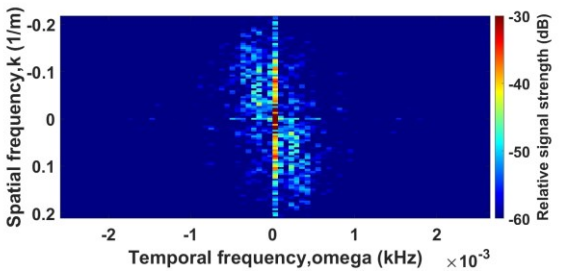

(b)

Fig. 7. ω-k plots generated from selected regions of the range-time intensity plots in Fig. 3 (a) for 94 GHz, and (b) for 24 GHz

C. ω-k Plot

Performing a 2D Fourier transformation of the range-intensity plot produces the ω-k plot, which is useful to visualize the non-linear interaction in the wave dynamics [3]. The range-time intensity regions where significant periodic wave backscatter is evident in Fig. 3 (regions close to the rock) were chosen in favor of the more arbitrary wave patterns at closer ranges. For 94 GHz, the region covering 40-100 m was selected and for 24 GHz, 40-150 m was chosen. A larger range swath was selected for 24 GHz because of the larger range bins, so more samples were needed to maintain a similar spatial frequency resolution as the 94 GHz plot. Fig. 7(a) shows the processed ω-k plot for the 94 GHz data in log scale. The parabolic-like gravity wave dispersion line can be seen, corresponding to waves approaching the radar [3]. The associated dispersion line for waves moving away is also observed, corresponding to waves reflected off the rocks. The lesser signal strength and slightly different shape is also expected, as more waves are approaching than receding in the selected patch. Similar processing was done for the 24 GHz data as seen in Fig. 7(b), but the plot is less clear in this case, although still showing the dispersion line trend for the incoming waves. The reason for this is still not entirely understood and again can be further investigated.

V. CONCLUSION

This work has analysed the amplitude characteristics of various scattering components evident in littoral sea clutter data measured at 24 and 94 GHz. The data were obtained in very low sea-state and there was no measurable backscatter from the smooth sea surface (NRCS below -65 dB). However, sea spikes gave rise to strong signals and it was possible to differentiate the components contributing to the spikes in the radar returns. Bragg, burst and whitecap regions were carefully selected from the processed data and histograms of NRCS values were calculated for the given grazing angles. The modal NRCS value for Bragg scattering matches the updated NRL model quite well and lower NRCS values are observed at 24 GHz as expected, except from the Bragg scattering. This discrepancy should be the subject of more in-depth investigation. Additionally, power spectrum analyses of the range-time intensity plots were performed which successfully illustrated the various wave dynamic features.

As future work, more analysis on the amplitude data acquired during this trial will be conducted, specifically to explore the fit of a model to the amplitude distribution histograms as well as to determine the *ω-k* plot features which can be observed and how to relate these to wave dynamics. It is the broader goal of this project to update models for sea clutter using data which has previously been scarce in the frequency bands of interest. It is expected that as more datasets are collected at these frequencies and above W-band, for different sea-states during future trials, a more improved empirical sea clutter model will be developed.

ACKNOWLEDGMENT

This work was supported by the UK Engineering and Physical Sciences Research Council under grant EP/S032851/1.

REFERENCES

[1] F. Nathanson, J. P. Reilly, and M. N. Cohen, *Radar design principles : signal processing and the environment*. New York, 1969.

[2] V. Gregers-Hansen and R. Mital, "An improved empirical model for radar sea clutter reflectivity," *IEEE Trans. Aerosp. Electron. Syst.*, vol. 48, no. 4, pp. 3512–3524, 2012.

[3] K. Ward, R. Tough, and S. Watts, *Sea Clutter: Scattering, the K Distribution and Radar Performance*. Institution of Engineering and Technology, 2013.

[4] A. G. Stove, D. A. Robertson, and D. G. Macfarlane, "Littoral sea clutter returns at 94GHz," in *2014 International Radar Conference, Radar 2014*, 2014.

[5] B. X. Weidong Hu, Z. Li, Y. Liu, and Y. Zhao, "W-band Littoral Low Grazing Angle Sea Clutter Measurement," in *2019 IEEE International Conference on Computational Electromagnetics, ICCEM 2019 - Proceedings*, 2019.

[6] A. Danklmayer *et al.*, "Radar Propagation Experiment in the North Sea: The Sylt Campaign," *IEEE Trans. Geosci. Remote Sens.*, vol. 56, no. 2, pp. 835–846, Feb. 2018.

[7] S. Watts, K. D. Ward, and R. J. A. Tough, "The physics and modelling of discrete spikes in radar sea clutter," in *IEEE National Radar Conference - Proceedings*, 2005, vol. 2005-Janua, no. January, pp. 72–77.

[8] V. Corretja, J. Petitjean, J. M. Quellec, S. Kemkemian, H. Thuilliez, and S. Watts, "Sea-spike analysis in high range and Doppler resolution radar data," in *2014 International Radar Conference, Radar 2014*, 2014.

[9] D. A. Robertson, G. M. Brooker, and P. D. L. Beasley, "Very low-phase noise, coherent 94GHz radar for micro-Doppler and vibrometry studies," in *Proc. SPIE 9077, Radar Sensor Technology XVIII*, 2014, vol. 9077, p. 907719.

[10] S. Rahman and D. A. Robertson, "Coherent 24 GHz FMCW radar system for micro-Doppler studies," in *Proc. SPIE 10633, Radar Sensor Technology XXII*, 2018, no. 10633.

[11] L. Rosenberg, "Sea-spike detection in high grazing angle X-band sea-clutter," *IEEE Trans. Geosci. Remote Sens.*, vol. 51, no. 8, pp. 4556–4562, 2013.

[12] M. Greco, F. Gini, and M. Rangaswamy, "Statistical analysis of measured polarimetric clutter data at different range resolutions," *IEE Proc. Radar, Sonar Navig.*, vol. 153, no. 6, pp. 473–481, 2006.